arXiv:1408.3669v3 [cond-mat.str-el] 8 Jan 2015

Topology and Interactions in a Frustrated Slab: Tuning from Weyl Semimetals to $\mathcal{C} > 1$ Fractional Chern Insulators

E.J. Bergholtz[1], Zhao Liu[2], M. Trescher[1], R. Moessner[3], and M. Udagawa[4]
[1]*Dahlem Center for Complex Quantum Systems and Institut für Theoretische Physik, Freie Universität Berlin, Arnimallee 14, 14195 Berlin, Germany*
[2]*Department of Electrical Engineering, Princeton University, Princeton, New Jersey 08544, USA*
[3]*Max-Planck-Institut für Physik komplexer Systeme, Nöthnitzer Straße 38, D-01187 Dresden, Germany and*
[4]*Department of Applied Physics, University of Tokyo, Hongo 7-3-1, Bunkyo-ku, Tokyo 113-8656, Japan*
(Dated: January 9, 2015)

We show that, quite generically, a [111] slab of spin-orbit coupled pyrochlore lattice exhibits surface states whose constant energy curves take the shape of Fermi arcs, localized to different surfaces depending on their quasi-momentum. Remarkably, these persist independently of the existence of Weyl points in the bulk. Considering interacting electrons in slabs of finite thickness, we find a plethora of known fractional Chern insulating phases, to which we add the discovery of a new higher Chern number state which is likely a generalization of the Moore-Read fermionic fractional quantum Hall state. By contrast, in the three-dimensional limit, we argue for the absence of gapped states of the flat surface band due to a topologically protected coupling of the surface to gapless states in the bulk. We comment on generalizations as well as experimental perspectives in thin slabs of pyrochlore iridates.

PACS numbers: 73.43.Cd, 71.10.Fd, 73.21.Ac

Introduction.— The prediction [1–5] and subsequent experimental observation [6, 7] of topological insulators has fundamentally revolutionized the understanding of electronic states of matter during the past decade [8–10]. New frontiers in this field include gapless topological phases such as three-dimensional Weyl semimetals [11–15] exhibiting exotic Fermi arc surface states [13, 15–17], interaction effects on the gapless surface of topological insulators [18–22], and strongly correlated phases akin to fractional quantum Hall states in two-dimensional (2D) lattices (see Refs. [23, 24] and references therein). Drawing additional inspiration from the rapid development of growth techniques in fabricating high quality slabs/films/interfaces of oxide materials [25], this work provides intriguing connections between these seemingly disparate frontiers.

The materials pursuit for Weyl semimetals and its relatives is rapidly broadening [26–29], with spin-orbit coupled pyrochlore iridates, such as $Y_2Ir_2O_7$ [13, 30–32] being particularly promising compounds—as these are favourably grown/cleaved in the [111] direction, and given their predicted rich variety of strongly correlated phases [33, 34], we here study the surface bands of pyrochlore [111] slabs, where the system can be seen as a layered structure of alternating kagome and triangular layers [30] (Fig. 1).

Our work uncovers an intriguing dichotomy between bulk and surface states which allows us to establish connections between apparently disparate topological phenomena. While the bulk band structure changes drastically as a function of the inter-layer tunneling strength $t_\perp$—including the (dis)appearance of the Weyl semimetal—the surface states, which involve only the kagome layers, *remain unchanged* on account of their essentially geometrical origin. Most saliently, in the two distinct regimes of N weakly coupled kagome layers, each with unit Chern number, at small $t_\perp$, and the genuinely three-dimensional Weyl semimetal at large $t_\perp$, identical surface states carrying Chern number $\mathcal{C} = N$ are localized at opposite surfaces depending on their momentum. Constant energy contours in reciprocal space are Fermi arcs, which thus exist also in absence of Weyl nodes in the bulk!

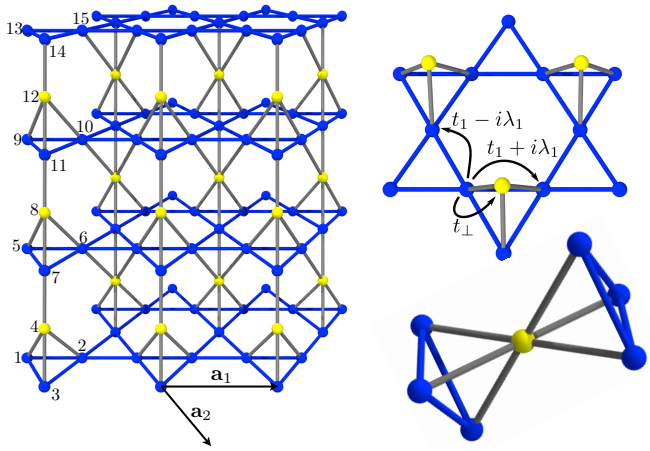

Figure 1. **The pyrochlore slab**. The left panel shows the [111] pyrochlore slab with $N = 4$ kagome layers (blue) separated by (yellow) sites of $N - 1 = 3$ triangular layers. A practical labeling of the $4N - 1 = 15$ sites in the unit cell and the basis vectors, $\mathbf{a}_1, \mathbf{a}_2$, of the Bravais lattice are also indicated. The top right panel indicates the considered nearest neighbor processes. The lower right panel shows the local environment of a triangular (yellow) site for which the local constraint of destructive interference directly leads to the surface states (1) at the heart of this work.

Upon adding interactions to a partially filled surface band—even when these are made very flat by tuning hopping

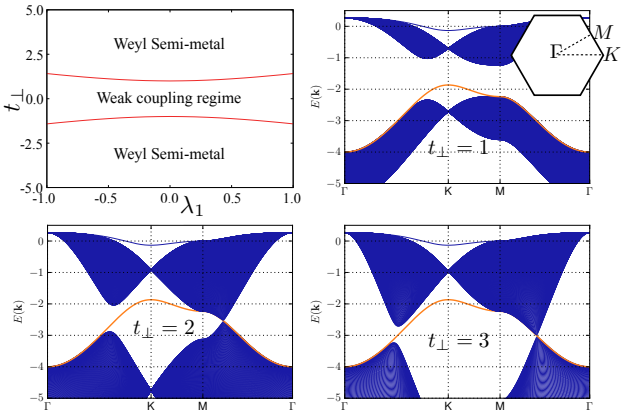

Figure 2. **Weakly coupled Chern insulators vs. Weyl semimetals**. As $t_\perp$ is increased there is a transition from a weakly-coupled regime to a distinct phase where Weyl nodes occur on the line connecting Γ and M. In the top left panel we show the phase diagram in the case of nearest neighbor hopping only (we set $t_1 = -1$ throughout) [36]. The other panels show example band structures with fixed $\lambda_1 = 0.5$ and varying $t_\perp = 1, 2, 3$ for a slab with $N = 300$ kagome layers along the crucial $\Gamma - K - M - \Gamma$ path through the projected 2D Brillouin zone (BZ) (cf. top right inset). Note that, remarkably, the band highlighted in orange corresponding to the surface states (2), is independent of $t_\perp$.

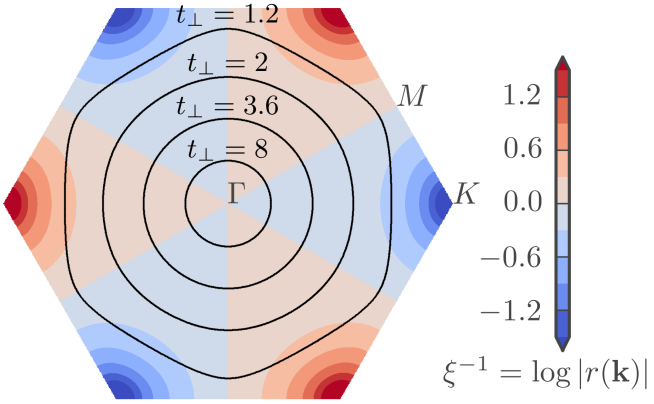

Figure 3. **Surface state structure and Fermi arcs**. The color scale indicates the inverse penetration depth, $\xi^{-1}(\mathbf{k}) = \log(|r(\mathbf{k})|)$ of the surface states throughout the 2D BZ for the same parameters, $t_1 = -1, \lambda_1 = 0.5$, used in Fig. 2. The black lines illustrate Fermi arcs for a chemical potential set at the Weyl node for a few $t_\perp$-values. When $\xi^{-1}(\mathbf{k})$ changes sign, the localization changes between top (red) to bottom (blue) surfaces, hence splitting the Fermi "circle" into six spatially disjoint arcs.

parameters—we argue that interactions do not open a gap for thick slabs, due to a leakage into the bulk along "soft" lines related to projections of remnant Weyl nodes. However, in thin slabs we find a plethora of possible fractionalized phases, some of which were discovered earlier [33, 34] with the implicit assumption of sub-critical inter-layer tunneling. Most prominently, we provide evidence for a first non-Abelian fermionic fractional Chern insulator (FCI) in a $\mathcal{C} > 1$ band, namely a $\mathcal{C} = 2$ generalization of the Moore-Read quantum Hall phase [35]. Our work thus gives a unifying and fresh perspective on the intriguing combination of fractionalization and topological surface localization impossible in strictly two-dimensional systems.

Setup.— Our tight binding model on N kagome layers, $\mathcal{K}_m$, alternating with $N-1$ triangular layers, $\mathcal{T}_m$ [30] (Fig. 1), considers spinless, spin-orbit coupled, fermions with interlayer hopping amplitude $t_\perp$ and kagome layer (next) nearest hopping amplitudes $t_1 \pm i\lambda_1$ ($t_2 \pm i\lambda_2$), where the $-(+)$ sign applies for (anti-)clockwise hopping w.r.t. the hexagon on which it takes place. Time-reversal symmetry is absent, e.g. due to an orbital field or spontaneous ferromagnetism.

Band structure and surface wave functions.— Independently of the form of the Bloch states of a single kagome layer, three bands of the N-layer system are exactly described by

$$|\psi^i(\mathbf{k})\rangle = \mathcal{N}(\mathbf{k}) \sum_{m=1}^{N} \Big(r(\mathbf{k})\Big)^m |\phi^i(\mathbf{k})\rangle_m \,, \qquad (1)$$

where $|\phi^i(\mathbf{k})\rangle_m$, $i = 1, 2, 3$ are the single layer Bloch states localized to $\mathcal{K}_m$ and $\mathcal{N}(\mathbf{k})$ ensures proper normalization. The coefficients $r(\mathbf{k})$ are determined by demanding that the amplitudes for hopping to the triangular layers vanish by interfering destructively (Fig. 1): $r(\mathbf{k}) = -\frac{\phi_1^i(\mathbf{k})+\phi_2^i(\mathbf{k})+\phi_3^i(\mathbf{k})}{e^{-ik_2}\phi_1^i(\mathbf{k})+e^{i(k_1-k_2)}\phi_2^i(\mathbf{k})+\phi_3^i(\mathbf{k})}$, where $\phi_n^i(\mathbf{k})$, $n \leq 3$, are the components of the Bloch spinor for the pertinent state $|\phi^i(\mathbf{k})\rangle$ in a single kagome-layer, and $k_{1,2} = \mathbf{k} \cdot \mathbf{a}_{1,2}$. While $\phi_n^i(\mathbf{k})$, $n \leq 3$, can be analytically obtained by diagonalizing 3×3 Hermitian matrices, the full Bloch spinor is fully known via $\psi_{4m}^i(\mathbf{k}) = 0$, $\psi_{n+4(m-1)}^i(\mathbf{k}) = \mathcal{N}(\mathbf{k})\big(r(\mathbf{k})\big)^m \phi_n^i(\mathbf{k})$ for all $\mathbf{k}, n, m$, with $E(\mathbf{k})$ of the states (1) equal to those of the single layer case.

Let us emphasize that, firstly, the states on the slab are exponentially localized to either the top or bottom layers, except in high symmetry cases where $|r(\mathbf{k})| = 1$. And secondly, if periodic boundary conditions are applied also in the [111]-direction, there are *no* generic eigenstates of the form (1), underscoring their surface nature.

In the following, we consider the case of single layer kagome bands carrying non-zero Chern number [44–46], say $\mathcal{C} = 1$. Then, the multilayer state (1) has Chern number N:

$$|\psi^{\mathcal{C}=N}(\mathbf{k})\rangle = \mathcal{N}(\mathbf{k}) \sum_{m=1}^{N} \Big(r(\mathbf{k})\Big)^m |\phi^{\mathcal{C}=1}(\mathbf{k})\rangle_m \qquad (2)$$

where $|\phi^{\mathcal{C}=1}(\mathbf{k})\rangle_m$ is the state localized to $\mathcal{K}_m$. The states (2) play a prominent role in this work, and their corresponding energies are highlighted in bold orange throughout this work (not shown are the two related states with $\mathcal{C} = 0, -N$).

Fig. 2 illustrates the finite $t_\perp$ transition between weakly coupled Chern insulators and the Weyl semimetal regime with linear band touching points described by

$$H_{\text{Weyl}} = \sum_i v_i \sigma_i k_i + E_0(\mathbf{k})\mathbb{I} \,, \qquad (3)$$

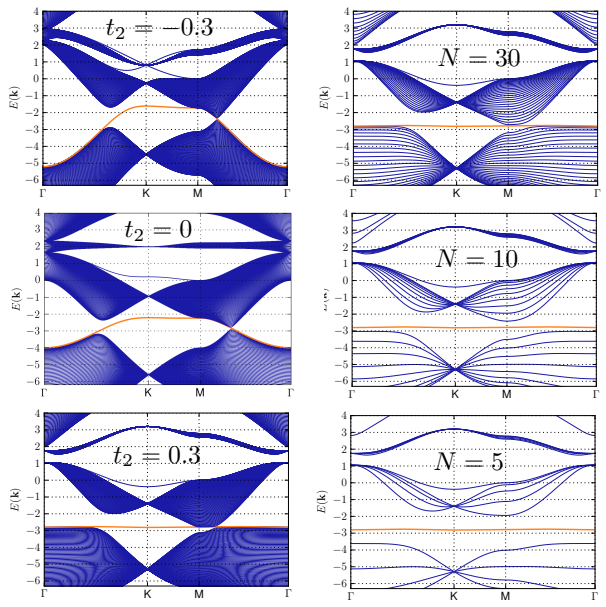

Figure 4. **From Weyl nodes to flat surface bands**. For $t_1 = -1, \lambda_1 = 0.3, \lambda_2 = 0.2, t_\perp = 2.0$, we plot the energy dispersion for various N and t_2 on the path $\Gamma - K - M - \Gamma$ through the BZ. In the left panel we set the number of kagome layers to $N = 100$ while varying t_2. For $t_2 = -0.3$ (top) there is a clearly visible Weyl node on the line connecting M and Γ. For $t_2 = 0$ the node is skewed and at $t_2 = 0.3$ it is essentially flattened while the surface band (bold orange) remains at almost fixed energy throughout the entire BZ. In the right panel we fix $t_2 = 0.3$ and reduce the number of layers, $N = 30, 10, 5$, from top to bottom, and a sizable finite size gap quickly opens throughout the entire BZ. The band highlighted in bold orange is that of (2), carrying Chern number $\mathcal{C} = N$.

where σ_i are Pauli matrices and $\mathbb{I}$ is the identity matrix. Precisely at the transition, the valence and conduction bands exhibit a two-fold degenerate touching at the M-points, which split into three pairs of (non-degenerate) Weyl cones that travel towards the Γ-point where they meet as $t_\perp \to \infty$. Remarkably, the states (2) are entirely independent of the value of $t_\perp$; in each case they describe states localized to the surfaces perpendicular to the [111] cleavage/cut/growth direction, while at the same time their interpretation fundamentally changes. Note also that the dispersion of the states (2) always traverses the Weyl point.

At fixed chemical potential, which may be fixed at the Weyl node due to stoichiometric considerations, the states (2) precisely describe Fermi arcs. In Fig. 3 we illustrate the momentum dependence of the surface localization of the states (2). Most saliently, we find that the penetration depth diverges along the lines connecting Γ and M. Crossing these lines, the localization changes between the bottom and top surfaces, which is the hallmark behavior of Fermi arcs. More specifically, a typical Fermi "circle" splits into six Fermi arcs which switch between top and bottom surface six times, whenever the Fermi circle crosses a Γ-M-line (cf. Fig. 3).

In Fig. 4 we go on to show how the state (2) can smoothly be transformed into a band which is essentially dispersionless, yet being tightly attached to bulk bands (for thick slabs). It is important to note that also the latter regime is described by a Weyl Hamiltonian (3) with a suitable choice of $E_0(\mathbf{k})$; the essential point is that the topology is unchanged as long as the band touching is linear ($v_i \neq 0, i = 1, 2, 3$), no matter how skewed the Weyl point is due to the overall constant dispersion $E_0(\mathbf{k})$. In fact, the Weyl nodes carry a quantized Chern flux and can as such only be annihilated by merging with an opposite chirality partner [15]. Furthermore, considering a quasi-two-dimensional slab, one finds that there is a fairly sizeable region in which the bandwidth is (much) smaller than the band gap, although to obtain very flat surface bands we need to include also next-nearest neighbor hopping (as done in Fig. 4). Crucially, this holds true for thin slabs both in the weakly coupled regime studied earlier [30, 33, 34], as well as when the bulk is in the Weyl semimetal regime.

Thus, one can consider the flat bands of Refs. [30, 33, 34] vestiges of Weyl semimetal surface bands. While $t_\perp$ considered in those works is slightly below the Weyl semimetal regime, our exact solution (2) reveals that this distinction is in fact immaterial in thin slabs as long as only the topological band is concerned.

Projected interactions in the flatbandlimit.– We now add interactions to a partially filled surface band with $\mathcal{C} = N$; for Weyl semimetals with the chemical potential pinned to the Weyl node in the bulk by stoichiometry, this may well be relevant to the low-energy physics of quasi-2D slabs.

The matrix elements of *any* local interaction (provided it is uniform throughout the lattice and does not couple different kagome layers) follows from (2); for a two-body interaction,

$$V^{\mathcal{C}=N}_{\mathbf{k}_1\mathbf{k}_2\mathbf{k}_3\mathbf{k}_4} = V^{\mathcal{C}=1}_{\mathbf{k}_1\mathbf{k}_2\mathbf{k}_3\mathbf{k}_4} \Big(\frac{|r(\mathbf{k}_1)|^2 - 1}{|r(\mathbf{k}_1)|^{2N} - 1} \cdots \frac{|r(\mathbf{k}_4)|^2 - 1}{|r(\mathbf{k}_4)|^{2N} - 1} \Big)^{\frac{1}{2}} \times \frac{(r^*(\mathbf{k}_1) r^*(\mathbf{k}_2) r(\mathbf{k}_3) r(\mathbf{k}_4))^N - 1}{r^*(\mathbf{k}_1) r^*(\mathbf{k}_2) r(\mathbf{k}_3) r(\mathbf{k}_4) - 1} \tag{4}$$

where the band projected interaction Hamiltonian in general can be written as

$$H_{\text{int}} = \sum_{\mathbf{k}_1\mathbf{k}_2\mathbf{k}_3\mathbf{k}_4} V^{\mathcal{C}=N}_{\mathbf{k}_1\mathbf{k}_2\mathbf{k}_3\mathbf{k}_4} c^\dagger_{\mathbf{k}_1} c^\dagger_{\mathbf{k}_2} c_{\mathbf{k}_3} c_{\mathbf{k}_4} \,, \tag{5}$$

where $c^\dagger_{\mathbf{k}}$ ($c_{\mathbf{k}}$) creates (annihilates) an electron in the state $|\psi^{\mathcal{C}=N}(\mathbf{k})\rangle$. These expressions generalize straightforwardly to any local $(k+1)-$body interaction. It is important to note that both the magnitude and the the relative phase factors of the matrix elements depend non-trivially on N.

Fractional topological phases.– The flat bands in our model [30] are known to host series of FCIs in bands with $\mathcal{C} > 1$: stable Abelian FCIs of fermions at band filling $\nu = \frac{1}{2\mathcal{C}+1}$ and bosons at $\nu = \frac{1}{\mathcal{C}+1}$ [33] with non-Abelian phases of bosons at $\nu = \frac{k}{\mathcal{C}+1}$ using onsite $(k+1)$-body interactions [34].

Here, we identify a new FCI at filling fraction $\nu = 1/3$, which we propose as a candidate for the first non-Abelian Fermionic FCI for $\mathcal{C} = 2$, a generalization of the Moore-Read quantum Hall state [35]. This is based on its large and robust

9-fold topological degeneracy (Fig. 5), its non-trivial entanglement spectra [36] as well as its provenance from a three-body interaction (see [36] for details). We note that, given the flat band is not located at the bottom of the spectrum, this state is indeed naturally suited to fermions at an appropriate density.

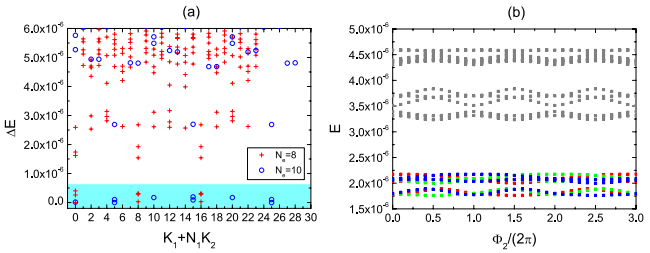

Figure 5. **Topological degeneracy in the $\mathcal{C} = 2$ bilayer system.** (a) The energy spectra of the interaction $H = \sum_{\langle i,j,k\rangle} n_i n_j n_k$ interaction projected to the flatbandfor $N_e = 8$ and $N_e = 10$ electrons in lattices with $N_1 \times N_2 = (N_e/2) \times 6$ unit cells yielding a filling fraction of $\nu = 1/3$. Each energy level is labeled by the conserved many-body momentum (K_1, K_2). The shaded area indicates the 9 quasi-degenerate states. (b) The y-direction spectral flow for 8 electrons under twisted boundary conditions $\Psi(\mathbf{r}_j + N_2\mathbf{a}_2) = \exp(i\Phi_2)\Psi(\mathbf{r}_j)$ of the ground state $\Psi(\mathbf{r}_j)$. The red, green and blue dots represent the 9 quasi-degenerate states in different momentum sectors, and the gray dots represent the excited states. The parameters are $t_1 = -1, \lambda_1 = 0.9, t_2 = \lambda_2 = 0$.

Gapless bulk.– Next, we argue that generically, a flat surface band will not be gapped by interactions within it for thick slabs. This happens because of the – topologically stable – locations on lines in reciprocal space where the states of the band switch the surface at which they are localised. At these points, the inverse penetration depth $\xi^{-1}(\mathbf{k}) = \log(|r(\mathbf{k})|)$ (cf. Fig. 3) vanishes. Matrix elements $V^{\mathcal{C}=N}_{\mathbf{k}_1\mathbf{k}_2\mathbf{k}_3\mathbf{k}_4}$ involving $n_{\{k_i\}}$ momenta on these lines vanish as $\left(\frac{1}{\sqrt{N}}\right)^{n_{\{k_i\}}}$, reflecting the spatial spread of the wavefunctions.

This is borne out by our numerics, where the absence of a FCI is indicated by an inhomogeneous electron distribution $n(\mathbf{k})$ in reciprocal space, reminiscent of a Fermi surface (Fig. 6). This is analogous to the compressible states at high filling fractions in $\mathcal{C} = 1$ bands, where an effective "hole-dispersion", $E_h(\mathbf{k})$ [36], resulting from a particle-hole transformation, dictates the low-energy physics [38]. In fact, both $\xi^{-1}(\mathbf{k})$ and $E_h(\mathbf{k})$ correlate rather well with $n(\mathbf{k})$ as illustrated for $\nu = 1/3$ with nearest neighbor repulsion, $H = \sum_{\langle i,j\rangle} n_i n_j$ (Fig. 6, see the supplementary materials for details and further examples [36]).

Discussion.— In this work, we have unraveled a striking connection between seemingly distinct frontiers of contemporary condensed matter physics by explicitly demonstrating that flat bands with Chern number $\mathcal{C} = N$ appearing on a slab of pyrochlore [30], and known to harbor a rich variety of fractional Chern insulators [33, 34], are in fact surface state vestiges of the Fermi arcs of Weyl semimetals [13]. This result has a bearing in the general context of the bulk-boundary correspondence in topological matter: while it has been realized that there can be phase transitions on the boundary while leaving the bulk intact [47, 48], we find a striking example of the converse situation with a bulk transition leaving the boundary theory unaffected.

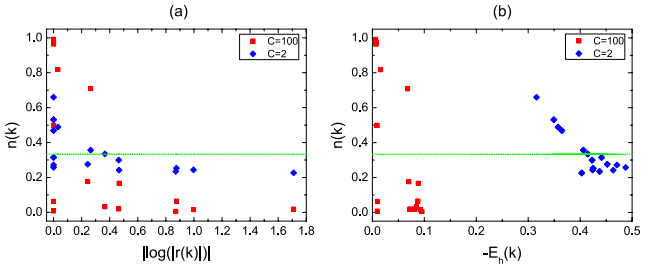

Figure 6. **Ground state occupation numbers.** $n(\mathbf{k})$ plotted against $|\xi(r(\mathbf{k}))|^{-1} = |\log(|r(\mathbf{k})|)|$ (left panel) and $-E_h(\mathbf{k})$ (right panel, cf. Ref. [38]) for Chern numbers $\mathcal{C} = 2$ (blue diamond) and $\mathcal{C} = 100$ (red square) at $\nu = 1/3$. This illustrates a general trend: $n(\mathbf{k})$ generically very inhomogenous at large $\mathcal{C}$ while it can remain comparably constant for small $\mathcal{C}$ (and ν) [36].

We note that layered structures, albeit with a rather different alternating normal insulator-strong topological insulator setup, have been suggested earlier as a possible platform for Weyl semimetals [14, 49]. Weyl semi-metals have also been predicted to occur in pyrochlore based bulk materials, in particular in $A_2Ir_2O_7$ (A is a rare-earth element) iridates [13], for which the existence of remnant Fermi arc states at certain magnetic domain walls even in the absence of bulk Weyl nodes was recently suggested [17]. Given the experimental advantages with finite pyrochlore slabs grown in the [111] directions [30–32], as compared to other oxide interfaces such as perovskite heterostructures (which may also harbor intriguing flat bands [50, 51]), and the generality of our exact solutions for the surface states based solely on locality and lattice geometry, our setup has its distinct advantages even before considering intricate interaction effects.

The exact solutions (1,2) provide a generic recipe for "engineering" exotic surface states: coupling Chern insulators with a desirable, e.g. flat, dispersion [52] in a geometrically frustrated manner results in states with the same dispersion but with higher Chern number and added complexity of Fermi arc variety. While we focused on pyrochlore slabs, this procedure generalizes to other frustrated lattices.

We have also explored the effect of interactions in these bands and identified new fractionalized topological phases as well as generic gapless states as $\mathcal{C} \to \infty$. Our work establishes that the combined fractionalization and topological surface localization of the interacting states found here, and in Refs. [33, 34], are impossible in strictly two-dimensional (isotropic) models just as Fermi arcs cannot exist in purely two-dimensional band materials. This feature distinguishes the pyrochlore based FCIs from other $\mathcal{C} > 1$ generalizations of multilayer quantum Hall states [53–61].

The present work invites a number of interesting questions

regarding the interplay between fractionalization, surface localization and translation symmetry. In this context, it would be particularly interesting to investigate the effects of lattice dislocations [53, 62].

We thank J. Behrmann and A. Läuchli for related collaborations. EJB is grateful to P. Brouwer, T. Ojanen and B. Sbierski for numerous discussions on Weyl semi-metals. EJB and MT are supported by DFG's Emmy Noether program (BE 5233/1-1). Z. L. is supported by the Department of Energy, Office of Basic Energy Sciences, through Grant No. DE-SC0002140. M. U. is supported by Grants-in-Aid for Scientific Research (No. 24340076, 26400339, and 24740221). This work was in part supported by the Helmholtz VI "New States of Matter and Their Excitations".

[1] C. L. Kane and E. J. Mele, *Quantum Spin Hall Effect in Graphene*, Phys. Rev. Lett. **95**, 226801 (2005).
[2] B.A. Bernevig, T-L Hughes and S.-C. Zhang, *Quantum Spin Hall Effect and Topological Phase Transition in HgTe Quantum Wells*, Science **314**, 1757 (2006).
[3] J. E. Moore and L. Balents, *Topological invariants of time-reversal-invariant band structures*, Phys. Rev. B **75**, 121306 (2007).
[4] L. Fu, C. L. Kane, and E. J. Mele, *Topological Insulators in Three Dimensions*, Phys. Rev. Lett. **98**, 106803 (2007).
[5] R. Roy, *Topological phases and the quantum spin Hall effect in three dimensions*, Phys. Rev. B **79**, 195322 (2009).
[6] M. König, *et. al.*, *Quantum Spin Hall Insulator State in HgTe Quantum Wells*, Science **318**, 766 (2007).
[7] D. Hsieh, D. Qian, L. Wray, Y. Xia, Y. S. Hor, R. J. Cava, and M. Z. Hasan, *A topological Dirac insulator in a quantum spin Hall phase*, Nature **452**, 970 (2008).
[8] M. Z. Hasan and C. L. Kane, *Colloquium: Topological insulators*, Rev. Mod. Phys. **82**, 3045 (2010).
[9] X.-L. Qi and S.-C. Zhang, *Topological insulators and superconductors*, Rev. Mod. Phys. **83**, 1057 (2011).
[10] B. A. Bernevig and T. L. Hughes, *Topological Insulators and Topological Superconductors* (Princeton University Press, Princeton, NJ, 2013).
[11] G. E. Volovik, *The Universe in a Helium Droplet* (Clarendon, Oxford, 2003).
[12] S. Murakami, *Phase transition between the quantum spin Hall and insulator phases in 3D: emergence of a topological gapless phase*, New J. Phys. **9**, 356 (2007).
[13] X. Wan, A. M. Turner, A. Vishwanath, and S. Y. Savrasov, *Topological semimetal and Fermi-arc surface states in the electronic structure of pyrochlore iridates*, Phys. Rev. B **83**, 205101 (2011).
[14] A. A. Burkov and L. Balents, *Weyl Semimetal in a Topological Insulator Multilayer*, Phys. Rev. Lett. **107**, 127205 (2011).
[15] For reviews, see A.M. Turner and A. Vishwanath, *Beyond Band Insulators: Topology of Semi-metals and Interacting Phases*, arXiv:1301.0330 and P. Hosur and X. Qi, *Recent developments in transport phenomena in Weyl semimetals*, C. R. Physique **14**, 857 (2013).
[16] T. Ojanen, *Helical Fermi arcs and surface states in time-reversal invariant Weyl semimetals*, Phys. Rev. B **87**, 245112 (2013).
[17] Y. Yamaji and M. Imada, *Metallic Interface Emerging at Magnetic Domain Wall of Antiferromagnetic Insulator: Fate of Extinct Weyl Electrons*, Phys. Rev. X **4**, 021035 (2014).
[18] M. Sitte, A. Rosch and L. Fritz, *Interaction effects on almost flat surface bands in topological insulators*, Phys. Rev. B **88**, 205107 (2013).
[19] C. Wang, A. C. Potter and T. Senthil, *Gapped symmetry preserving surface state for the electron topological insulator*, Phys. Rev. B **88**, 115137 (2013).
[20] M. A. Metlitski, C. L. Kane and M. P. A. Fisher, *A symmetry-respecting topologically-ordered surface phase of* $3D$ *electron topological insulators*, arXiv:1306.3286.
[21] P. Bonderson, C. Nayak and X.-L. Qi, *A time-reversal invariant topological phase at the surface of a 3D topological insulator*, J. Stat. Mech. P09016 (2013).
[22] X. Chen, L. Fidkowski and A. Vishwanath, *Symmetry enforced non-Abelian topological order at the surface of a topological insulator* Phys. Rev. B **89**, 165132 (2014).
[23] E.J. Bergholtz and Z. Liu, *Topological Flat Band Models and Fractional Chern Insulators*, Int. J. Mod. Phys. B **27**, 1330017 (2013).
[24] S. A. Parameswaran, R. Roy, and S. L. Sondhi, *Fractional quantum Hall physics in topological flat bands*, C. R. Physique **14**, 816 (2013).
[25] J. Mannhart and D. G. Schlom, *Oxide Interfaces—An Opportunity for Electronics*, Science **327**, 1607 (2010).
[26] M. Neupane, S.-Y. Xu, R. Sankar, N. Alidoust, G. Bian, C. Liu, I. Belopolski, T.-R. Chang, H.-T. Jeng, H. Lin, A. Bansil, F. Chou M. Z. Hasan, *Observation of a three-dimensional topological Dirac semimetal phase in high-mobility Cd3As2*, Nat. Commun. **5**, 3786 (2014).
[27] S. Borisenko, Q. Gibson, D. Evtushinsky, V. Zabolotnyy, B. Büchner, and R. J. Cava, *Experimental Realization of a Three-Dimensional Dirac Semimetal*, Phys. Rev. Lett. **113**, 027603 (2014).
[28] Z. K. Liu, B. Zhou, Y. Zhang, Z. J. Wang, H. M. Weng, D. Prabhakaran, S.-K. Mo, Z. X. Shen, Z. Fang, X. Dai, Z. Hussain, and Y. L. Chen, *Discovery of a Three-Dimensional Topological Dirac Semimetal, Na3Bi*, Science **343**, 864 (2014).
[29] H.-J. Kim, K.-S. Kim, J.-F. Wang, M. Sasaki, N. Satoh, A. Ohnishi, M. Kitaura, M. Yang, and L. Li, *Dirac versus Weyl Fermions in Topological Insulators: Adler-Bell-Jackiw Anomaly in Transport Phenomena*, Phys. Rev. Lett. **111**, 246603 (2013).
[30] M. Trescher and E. J. Bergholtz, *Flat bands with higher Chern number in pyrochlore slabs*, Phys. Rev. B **86**, 241111(R) (2012).
[31] X. Hu, A. Rüegg, and G. A. Fiete, *Topological phases in layered pyrochlore oxide thin films along the* $[111]$ *direction*, Phys. Rev. B **86**, 235141 (2012).
[32] B.-J. Yang and N. Nagaosa, *Emergent Topological Phenomena in Thin Films of Pyrochlore Iridates*, Phys. Rev. Lett. **112**, 246402 (2014).
[33] Z. Liu, E.J. Bergholtz, H. Fan, and A.M. Läuchli, *Fractional Chern Insulators in Topological Flat bands with Higher Chern Number*, Phys. Rev. Lett. **109**, 186805 (2012).
[34] A. Sterdyniak, C. Repellin, B. Andrei Bernevig, and N. Regnault, *Series of Abelian and non-Abelian states in* $C > 1$ *fractional Chern insulators*, Phys. Rev. B **87**, 205137 (2013).
[35] G. Moore, and N. Read, *Nonabelions in the fractional quantum Hall effect*, Nucl. Phys. B **360**, 362 (1991).
[36] See the Supplemental Material, which includes Refs. [2, 4–8, 30, 38], for more details.
[37] N. R. Cooper, N. K. Wilkin, and J. M. F. Gunn, *Quantum Phases of Vortices in Rotating Bose-Einstein Condensates*, Phys.

Rev. Lett. **87**, 120405 (2001).
[38] A.M. Läuchli, Z. Liu, E.J. Bergholtz, and R. Moessner, *Hierarchy of fractional Chern insulators and competing compressible states*, Phys. Rev. Lett. **111**, 126802 (2013).
[39] N. Regnault and B. A. Bernevig, *Fractional Chern Insulator*, Phys. Rev. X **1**, 021014 (2011).
[40] A. Sterdyniak, N. Regnault, and B. A. Bernevig, *Extracting Excitations from Model State Entanglement*, Phys. Rev. Lett. **106**, 100405 (2011).
[41] M. Greiter, X.-G. Wen, and F. Wilczek, *Paired Hall state at half filling*, Phys. Rev. Lett. **66**, 3205 (1991).
[42] B.A. Bernevig and N. Regnault, *Emergent many-body translational symmetries of Abelian and non-Abelian fractionally filled topological insulators*, Phys. Rev. B **85**, 075128 (2012).
[43] Y.-F. Wang, H. Yao, Z.-C. Gu, C.-D. Gong, and D. N. Sheng, *Non-Abelian Quantum Hall Effect in Topological Flat Bands*, Phys. Rev. Lett. **108**, 126805 (2012).
[44] F.D.M. Haldane, *Model for a Quantum Hall Effect without Landau Levels: Condensed-Matter Realization of the "Parity Anomaly"*, Phys. Rev. Lett. **61**, 2015 (1988).
[45] E. Tang, J.-W. Mei, and X.-G. Wen, *High-Temperature Fractional Quantum Hall States*, Phys. Rev. Lett. **106**, 236802 (2011).
[46] Z.-X. Liu, J.-W. Mei, P. Ye, and X.-G. Wen, $U(1) \times U(1)$ *Symmetry Protected Topological Order in Gutzwiller Wave Functions*, arXiv:1408.1676.
[47] J. Cano, M. Cheng, M. Mulligan, C. Nayak, E. Plamadeala, and J. Yard, *Bulk-edge correspondence in (2+1)-dimensional Abelian topological phases*, Phys. Rev. B **89**, 115116 (2014).
[48] A. Chandran, V. Khemani, and S.L. Sondhi, *How Universal Is the Entanglement Spectrum?*, Phys. Rev. Lett. **113**, 060501(2014).
[49] A. A. Burkov, M. D. Hook, and L. Balents, *Topological nodal semimetals*, Phys. Rev. B **84**, 235126 (2011).
[50] D. Xiao, W. Zhu, Y. Ran, N. Nagaosa, and S. Okamoto, *Interface engineering of quantum Hall effects in digital transition metal oxide heterostructures*, Nat. Commun. **2**, 596 (2011).
[51] F. Wang and Y. Ran, *Nearly flat band with Chern number* $C = 2$ *on the dice lattice*, Phys. Rev. B **84**, 241103(R) (2011).
[52] E. Kapit and E. Mueller, *Exact Parent Hamiltonian for the Quantum Hall States in a Lattice*, Phys. Rev. Lett. **105**, 215303 (2010).
[53] M. Barkeshli and X.-L. Qi, *Topological Nematic States and Non-Abelian Lattice Dislocations*, Phys. Rev. X **2**, 031013 (2012).
[54] Y.-F. Wang, H. Yao, C.-D. Gong, and D. N. Sheng, *Fractional Quantum Hall Effect in Topological Flat Bands with Chern Number Two*, Phys. Rev. B **86**, 201101(R) (2012).
[55] S. Yang, Z.-C. Gu, K. Sun, and S. Das Sarma, *Topological flat band models with arbitrary Chern numbers*, Phys. Rev. B **86**, 241112(R) (2012).
[56] L. Hormozi, G. Moller, and S. H. Simon, *Fractional Quantum Hall Effect of Lattice Bosons Near Commensurate Flux*, Phys. Rev. Lett. **108**, 256809 (2012).
[57] A. G. Grushin, T. Neupert, C. Chamon, and C. Mudry, *Enhancing the stability of fractional Chern insulators against competing phases*, Phys. Rev. B **86**, 205125 (2012).
[58] Y.-L Wu, N. Regnault, and B. A. Bernevig, *Bloch Model Wave Functions and Pseudopotentials for All Fractional Chern Insulators*, Phys. Rev. Lett. **110**, 106802 (2013).
[59] D. Wang, Z. Liu, J. Cao, and H. Fan, *Tunable Band Topology Reflected by Fractional Quantum Hall States in Two-Dimensional Lattices*, Phys. Rev. Lett. **111**, 186804 (2013).
[60] Y.-H. Wu, J. K. Jain, and K. Sun, *Fractional Topological Phases in Generalized Hofstadter Bands with Arbitrary Chern Numbers*, arXiv:1309.1698.
[61] M. Udagawa and E.J. Bergholtz, *Correlations and entanglement in flat band models with variable Chern numbers*, J. Stat. Mech. P10012 (2014).
[62] Y. Ran, Y. Zhang and A. Vishwanath, *One-dimensional topologically protected modes in topological insulators with lattice dislocations*, Nature Physics **5**, 298 (2009).

SUPPLEMENTARY MATERIAL

In this supplementary material we present a more exhaustive single particle phase diagram of the pyrochlore slab model, and provide additional details and data for the interacting flat band problem to illustrate the contrasting behavior in thin and thick slabs. Our data corroborate our conclusion of the absence of insulating states in the flat surface bands of very thick slabs, i.e. at very large Chern numbers, where the occupation numbers $n(\mathbf{k})$ are generically inhomogeneous and feature Fermi surface-like kinks, which are characteristic of the predicted gapless states. Finally, we present entanglement spectra and some general arguments in favor of the non-Abelian interpretation of the discovered $\nu = 1/3, \mathcal{C} = 2$ fractional Chern insulator.

Single particle phase diagram

We begin this supplementary material by providing a more complete single particle phase diagram for the pyrochlore slab model [S1], as shown in Fig. S1. Compared to the phase diagram presented in the main text, this phase diagram covers a wider range of parameter values, and despite the simplicity of the model, we find that the phase diagram has a quite rich structure. In total there are five different bulk phases present for generic nearest neighbor parameters, $t_\perp, \lambda_1$ (we keep $t_1 = -1$ fixed). Each phase has distinct nature of bulk single-particle excitation gaps at quarter filling. The excitation gap is obtained by assuming periodic boundary conditions for all three directions.

To describe the main features of the phase diagram, we firstly note that the energy spectrum is symmetric under the transformation $\lambda \leftrightarrow -\lambda$ and $t_\perp \leftrightarrow -t_\perp$, so we can focus on the region $\lambda_1 \geq 0$ and $t_\perp \geq 0$ without loss of generality. Let us start with fixing $t_\perp = 0$. In this case, the system is basically insulating at quarter filling, with a finite excitation gap. However, there are two exceptional points: $\lambda_1 = 0$ and $\lambda_1 = \sqrt{3}$, where the system becomes gapless. These two points may be termed as quantum critical points, which separate two insulating regions. The region of small λ: $0 \leq \lambda_1 \leq \sqrt{3}$ corresponds to the parameter space we focus on in the main text. As increasing $t_\perp$, the system turns into a Weyl semi-metal (WS) in this region, signaled by the touching of lowest and second-lowest energy bands, as is discussed in the main text.

More complicated changes can be observed for larger λ_1 region: $\lambda_1 \geq \sqrt{3}$. In this case, as increasing $t_\perp$, the energy gap

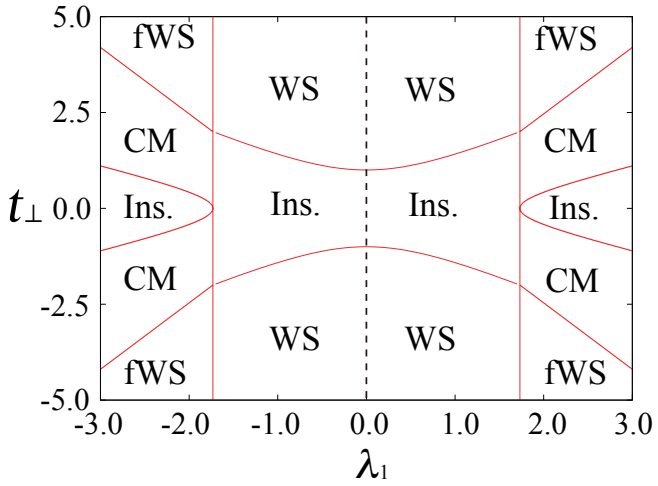

Figure S1. The complete nearest-neighbour phase diagram of the pyrochlore slab model [S1], which is composed of the insulating region (Ins.), the Weyl semi-metal phase (WS), compensated metallic phase (CM), and the flat Weyl semi-metal phase (fWS). For the characterization of fWS phase, see the text below. The dashed line at $\lambda_1 = 0$ means the line degeneracy ("line node") remains along this line.

closes indirectly. In other words, the top of lowest band and the bottom of second-lowest band exist at different momenta, and they exhibit a level crossing. This leads to the formation of Fermi surfaces with the same density of electron-like and hole-like carriers; the system enters a compensated metallic (CM) phase.

Within the CM phase, the direct gap also closes on increasing $t_\perp$, and the Weyl nodes show up, even though the existence of bulk carriers masks the influence of small carrier density around Weyl nodes. However, as increasing $t_\perp$ further, Fermi surfaces disappear, and another Weyl semi-metal phase appears. This WS phase has a distinct feature that the Weyl cones are extremely tilted so that one of the conical generatrix of the Weyl cone becomes horizontal. This leads to the line-like Fermi node, rather than Fermi points, and gives finite density of states at Fermi level, in contrast to the ordinary WS phase. We term this WS phase as "flat Weyl semi-metal", and distinguish it from the WS phase for small λ_1.

Gapless three-dimensional limit

Below we will elaborate on the inability of interactions to open up a gap in the three-dimensional limit, $\mathcal{C} = N \to \infty$.

Compressibility.— A useful quantity to consider is

$$\Delta(N_e) = N_e\Big[\frac{E_0(N_e+1)}{N_e+1} + \frac{E_0(N_e-1)}{N_e-1} - 2\frac{E_0(N_e)}{N_e}\Big],$$

which (usually called charge gap) is a measure of (inverse) compressibility [S2]. Here $E_0(N_e)$ is the ground energy of a system with N_e electrons. A clear hint of an incompressible state, such as a fractional Chern insulator, is the existence of a peak in $\Delta(N_e)$ at the pertinent filling fraction (assuming a fixed lattice size). In Fig. S2 we plot $\Delta(N_e)$ for a system with $N_1 \times N_2 = 6 \times 5$ unit cells and Chern number $\mathcal{C} = 2, 100$ (left panel) and $N_1 \times N_2 = 7 \times 4$ and $\mathcal{C} = 3, 200$ (right panel). The lattice sizes are deliberately chosen as to accommodate filling fractions of known FCIs ($\nu = 1/5$ for $\mathcal{C} = 2$ and $\nu = 1/7$ for the $\mathcal{C} = 3$ case), but the general arguments given below for the difference between large and small $\mathcal{C}$ are independent of the particular lattice chosen. Perhaps somewhat surprisingly, our plots show a large number of peaks, also at high Chern numbers. Below, we corroborate the arguments given in the main text, and argue that, while the small $\mathcal{C}$ peaks frequently corresponds to FCIs, the large $\mathcal{C}$ peaks, which are instable against flux insertion, are due to finite size effects rather than corresponding to FCIs. In passing, we note that some of the small $\mathcal{C}$ peaks present may correspond to FCIs not reported previously, but a detailed investigation thereof is left for future studies.

Hole-dispersion and penetration depth.— A striking feature of the compressibility plots (Fig. S2) is the particle-hole asymmetry. This is a direct consequence of the lack of translation invariance in the band. Following Ref. [S3], this is readily seen by performing a particle-hole transformation, $c_{\mathbf{k}} \to c^\dagger_{\mathbf{k}}$ within the band. Focusing on fermions, the projected Hamiltonian transforms to

$$\begin{aligned} H \;=\; & \sum_{\mathbf{k}_1,\mathbf{k}_2,\mathbf{k}_3,\mathbf{k}_4} V^{\mathcal{C}=N}_{\mathbf{k}_1\mathbf{k}_2\mathbf{k}_3\mathbf{k}_4} c^\dagger_{\mathbf{k}_1} c^\dagger_{\mathbf{k}_2} c_{\mathbf{k}_3} c_{\mathbf{k}_4} \to \\ \to & \sum_{\mathbf{k}_1,\mathbf{k}_2,\mathbf{k}_3,\mathbf{k}_4} \left(V^{\mathcal{C}=N}_{\mathbf{k}_1\mathbf{k}_2\mathbf{k}_3\mathbf{k}_4}\right)^* c^\dagger_{\mathbf{k}_1} c^\dagger_{\mathbf{k}_2} c_{\mathbf{k}_3} c_{\mathbf{k}_4} + \\ & + \sum_{\mathbf{k}} E_h(\mathbf{k}) c^\dagger_{\mathbf{k}} c_{\mathbf{k}}, \end{aligned}$$

which generates an effective single-hole dispersion

$$E_h(\mathbf{k}) = \sum_{\mathbf{m}} (V^{\mathcal{C}=N}_{\mathbf{mkmk}} + V^{\mathcal{C}=N}_{\mathbf{kmkm}} - V^{\mathcal{C}=N}_{\mathbf{kmmk}} - V^{\mathcal{C}=N}_{\mathbf{mkkm}}).$$

Within a Landau level, $E_h(\mathbf{k})$ is dispersionless (i.e. a chemical potential) while $E_h(\mathbf{k})$ is generically dispersive in a Chern band due to the breaking of translation invariance in reciprocal space.

That peaks in $\Delta(N_e)$ are only seen above $\nu = 1/2$ for large $\mathcal{C}$ is a clear sign that $E_h(\mathbf{k})$ is increasingly relevant for larger ν. As argued in Ref. [S3] for the case of large filling fractions in flat $\mathcal{C} = 1$ bands, a significant dispersion $E_h(\mathbf{k})$ leads to gapless states; the ground state is simply obtained by filling the states with largest $E_h(\mathbf{k})$, and such a state has Fermi surface(s) and supports gapless excitations in the thermodynamic limit. However, in a finite size lattice, this may result in sizable gaps which explain the peaks in $\Delta(N_e)$ occurring at large $\mathcal{C}$ and high filling fractions.

This connects nicely to the argument given in the main text for the generic existence of gapless excitations for large $\mathcal{C}$ by the fact that $E_h(\mathbf{k})$ tends to zero precisely when the penetration depth diverges (which occurs on the lines connecting Γ and M). In Fig. S3 we show precisely how $E_h(\mathbf{k})$ correlates

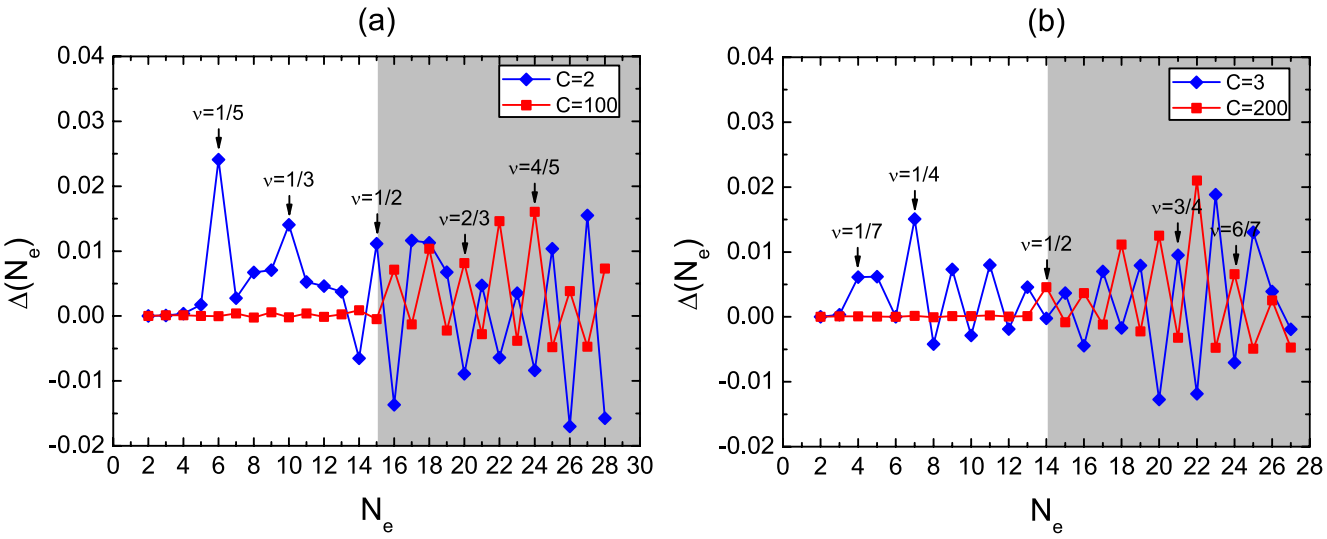

Figure S2. The discontinuity of chemical potential, $\Delta(N_e)$, plotted against electron number N_e in the (a) 6×5 and (b) 7×4 lattice. The parameters are $t_1 = -1, \lambda_1 = 1.1, t_2 = \lambda_2 = 0$.

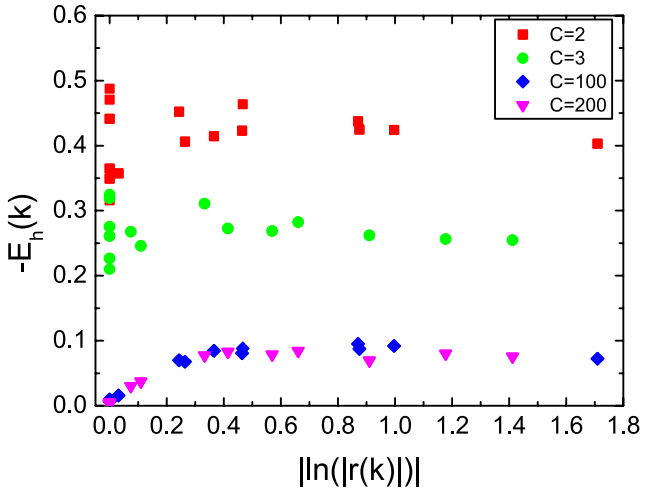

Figure S3. $-E_h(\mathbf{k})$ plotted against $|\xi(r(\mathbf{k}))| = |\log(|r(\mathbf{k})|)|$ for $\mathcal{C} = 2, 100$ ($N_1 \times N_2 = 6 \times 5$) and $\mathcal{C} = 3, 200$ ($N_1 \times N_2 = 7 \times 4$), with parameters $t_1 = -1, \lambda_1 = 1.1, t_2 = \lambda_2 = 0$.

with the inverse correlation length $|\xi(r(\mathbf{k}))| = |\log(|r(\mathbf{k})|)|$ for Chern numbers $\mathcal{C} = N = 2, 3, 100$ and 200.

Occupation number distributions.— The arguments given above and in the main text can be further tested by numerically diagonalizing the full interacting many-particle problem in a small finite size sample and then plotting $n(\mathbf{k})$ versus $|\xi(r(\mathbf{k}))| = |\log(|r(\mathbf{k})|)|$ as well as $E_h(\mathbf{k})$. In Figs. S4 and S5, we provide this for the system sizes, Chern numbers and filling fractions where we observe peaks in $\Delta(N_e)$ (cf. Fig. S2). We observe that $n(\mathbf{k})$ is only smooth and approximately constant at small Chern numbers $\mathcal{C}$ and filling fractions ν. At large ν we always find that $n(\mathbf{k})$ for a Fermi surface like feature when plotted against $-E_h(\mathbf{k})$; this holds true both for small and large Chern numbers. For small ν and large $\mathcal{C}$, we find that $n(\mathbf{k})$ also correlates strongly with $|\xi(r(\mathbf{k}))|$—it simply costs very little interaction energy to put further particles wherever $\xi(r(\mathbf{k}))$ diverges. That $n(\mathbf{k})$ is never close to being homogenous at any filling fraction for $\mathcal{C} = 100$ and 200—in each case there are orbitals with $n(\mathbf{k}) \approx 0$ and/or $n(\mathbf{k}) \approx 1$—is strongly corroborating our conclusion that the flat bands at large $\mathcal{C}$ generically remain gapless as interactions are turned on.

Further evidence for the generalized $\mathcal{C} = 2$ Moore-Read FCI

Entanglement spectrum.— In order to further elucidate the FCI character of $\nu = 1/3$ states stabilized by three-body interaction in $\mathcal{C} = 2$ band, we calculate the particle-cut entanglement spectrum (PES) [S4]. By dividing the system into N_A particles and $N_e - N_A$ particles, the information of the quasihole excitation is encoded in the spectrum of the reduced density matrix of part A. In Fig. S6, we show the PES for $N_e = 8$ electron with N_A from 2 to $N_e/2$. The fact that a number of levels exist below a clear gap in the PES for small N_A is sufficient to rule out the possible competing non-topological states such as charge density waves. Although the gap is invisible for the largest N_A, this is a situation often encountered in finite size studies, even in the case of very robust topological phases. Most notably, the PES gap is also absent even for the Coulomb ground state at $\nu = 1/3$ in the lowest Landau level [S5], which is a well-known fractional quantum Hall state in the Laughlin phase.

The PES data together with the topological degeneracy and spectral flow in the main text strongly support that the ground states are FCIs. The excitations of this phase are most likely non-Abelian as indicated by the high ground state degener-

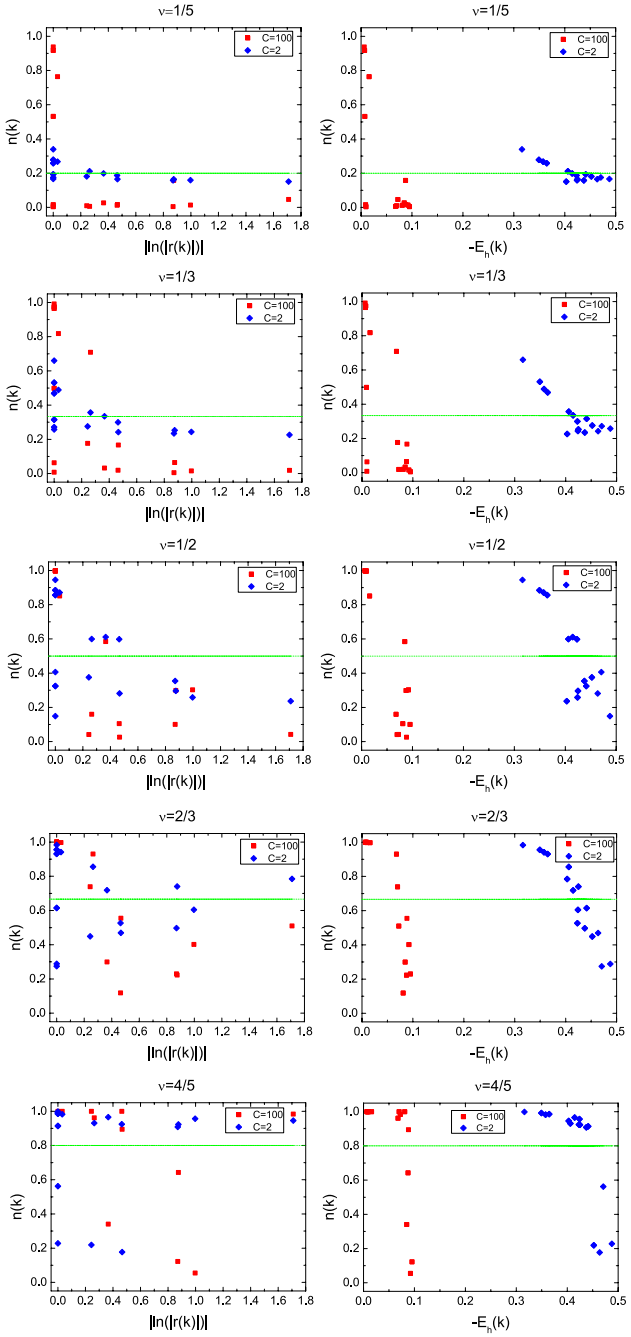

Figure S4. $n(\mathbf{k})$ plotted against $|\xi(r(\mathbf{k}))| = |\log(|r(\mathbf{k})|)|$ (left column) and $-E_h(\mathbf{k})$ (right column) for Chern numbers $C = 2$ (blue diamonds) and $C = 100$ (red squares) at various ν in the 6×5 lattice, with parameters $t_1 = -1, \lambda_1 = 1.1, t_2 = \lambda_2 = 0$. The green dotted lines indicate the reference $n(\mathbf{k}) = \nu$.

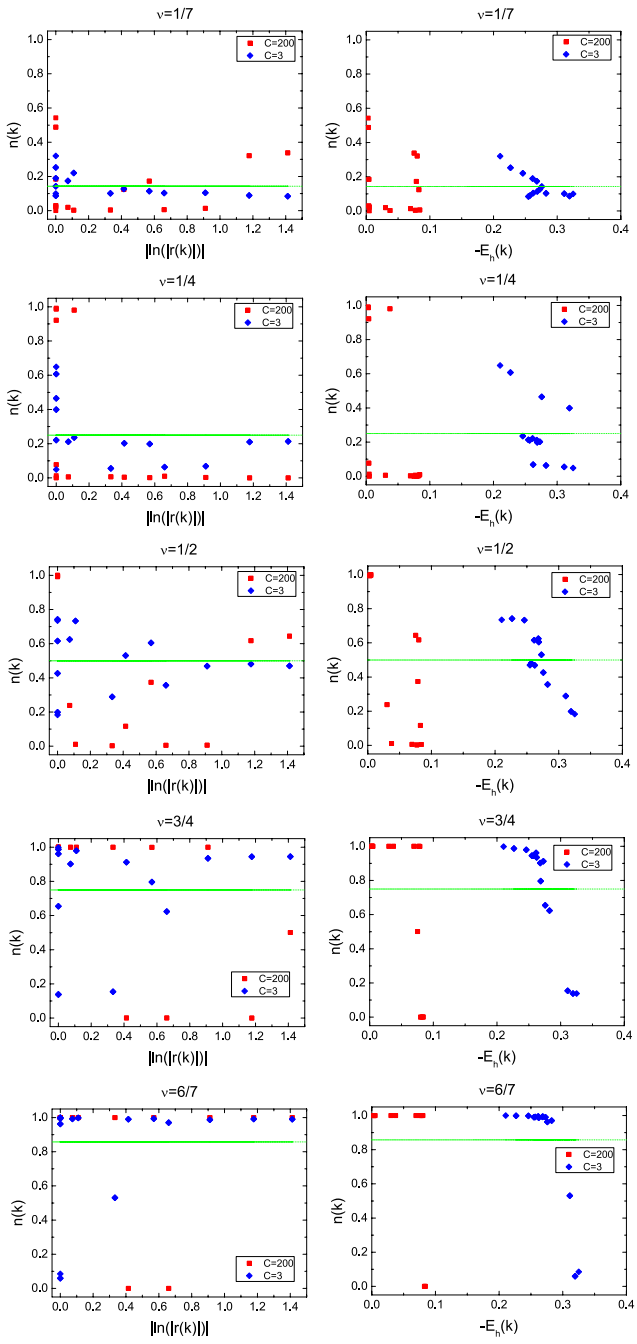

Figure S5. $n(\mathbf{k})$ plotted against $|\xi(r(\mathbf{k}))| = |\log(|r(\mathbf{k})|)|$ (left column) and $-E_h(\mathbf{k})$ (right column) for Chern numbers $C = 3$ (blue diamonds) and $C = 200$ (red squares) at various ν in the 7×4 lattice, with parameters $t_1 = -1, \lambda_1 = 1.1, t_2 = \lambda_2 = 0$. The green dotted lines indicate the reference $n(\mathbf{k}) = \nu$.

acy, and most saliently, by the local three-body constraint they originate from which is closely analogous to that of ordinary $\mathcal{C} = 1$ Moore-Read fractional quantum Hall states [S6] and their lattice analogues [S7, S8]. In this context we also note that a repulsive two-body interaction leads to another candidate FCI state at $\nu = 1/3, \mathcal{C} = 2$, which has also not been reported earlier, albeit with a three-fold degeneracy and, most likely, Abelian low energy excitations.

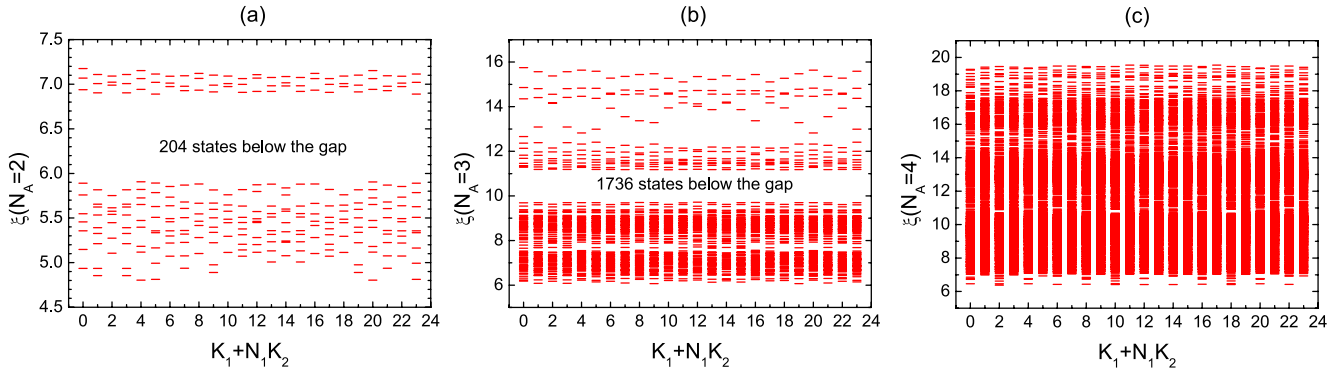

Figure S6. The particle-cut entanglement spectrum for $N_e = 8, N_1 \times N_2 = 4$ with three-body interaction at $\nu = 1/3$ in $\mathcal{C} = 2$ band. The parameters are $t_1 = -1, \lambda_1 = 0.9, t_2 = \lambda_2 = 0$.

[S1] M. Trescher and E. J. Bergholtz, *Flat bands with higher Chern number in pyrochlore slabs*, Phys. Rev. B **86**, 241111(R) (2012).

[S2] N. R. Cooper, N. K. Wilkin, and J. M. F. Gunn, *Quantum Phases of Vortices in Rotating Bose-Einstein Condensates*, Phys. Rev. Lett. **87**, 120405 (2001).

[S3] A.M. Läuchli, Z. Liu, E.J. Bergholtz, and R. Moessner, *Hierarchy of fractional Chern insulators and competing compressible states*, Phys. Rev. Lett. **111**, 126802 (2013).

[S4] N. Regnault and B. A. Bernevig, *Fractional Chern Insulator*, Phys. Rev. X **1**, 021014 (2011).

[S5] A. Sterdyniak, N. Regnault, and B. A. Bernevig, *Extracting Excitations from Model State Entanglement*, Phys. Rev. Lett. **106**, 100405 (2011).

[S6] M. Greiter, X.-G. Wen, and F. Wilczek, *Paired Hall state at half filling*, Phys. Rev. Lett. **66**, 3205 (1991).

[S7] B.A. Bernevig and N. Regnault, *Emergent many-body translational symmetries of Abelian and non-Abelian fractionally filled topological insulators*, Phys. Rev. B **85**, 075128 (2012).

[S8] Y.-F. Wang, H. Yao, Z.-C. Gu, C.-D. Gong, and D. N. Sheng, *Non-Abelian Quantum Hall Effect in Topological Flat Bands*, Phys. Rev. Lett. **108**, 126805 (2012).